A basic population balance model for fluid bed spray granulation

A.W. Vreman*[,a], C.E. van Lare[a], M.J. Hounslow[b]

[a] *AkzoNobel, Velperweg 76, 6824 BM Arnhem, The Netherlands*
[b] *Department of Chemical and Process Engineering, University of Sheffield, Mappin Street, Sheffield S1 3JD, United Kingdom*

Abstract

A basic population balance approach is developed for a granulation process in a fluid bed spray granulator. The particle size distribution predicted by the model is confirmed by plant data. Hence this model is considered to be useful to describe and optimize an industrial process. The model depends on a limited number of parameters (most of these factors can be measured or are known): the spray volume flux, the nucleation fraction (the fraction of the spray volume flux which leads to new particles formed), the nucleation particle diameter, the product withdrawal threshold diameter, and the product withdrawal rate. Analysis of the model reveals a steady state constraint; a steady state does not exist if the nucleation fraction is too large. For cases where the steady state does exist, the steady state particle size distribution is solved analytically. A numerical implementation of the model is used to illustrate the transient evolution of the process. The steady state solution appears to be stable for a constant nucleation fraction. However, if the nucleation fraction depends on the bed height the steady state can be unstable. Such a situation may occur if the spray inlet is near the height of the bed surface. Instead of convergence towards a steady state, the transient solution displays ongoing oscillatory behavior with an oscillation period of a number of hours. A linear stability analysis is performed to confirm the findings on the stability of the steady state.

Key words: Population balance, Particulate processes, Granulation, Fluidization, Stability, Mathematical modelling

1. Introduction

Product quality is related to the particle size distribution for many particulate products. Particulate products can be manufactured in various processes such as spray drying, mechanical granulation, and fluid bed granulation. The present work concerns processes where a fluid bed granulator is used. In a fluid bed granulator, a liquid is sprayed onto an already existing powder bed that is fluidized with air. The liquid partially evaporates, leaving a dry material and particles that have grown. Such particle growth can be the result of aggregation, where the liquid acts as a binder (e.g. Tan et al., 2006), or it can be the result of so-called onion growth, where the material is deposited onto the particles

*Corresponding author.
Email address: bert.vreman@akzonobel.com (A.W. Vreman)

Preprint of the paper published in Chemical Engineering Science, Vol 64, pp 4389-4398 (2009).

layer by layer (e.g. Heinrich et al., 2002). It is obvious that these processes influence the particle size distribution. The particle size distribution is a key function, which controls final product properties such as bulk density, powder flowability and dustiness. It is the aim of this work to link process conditions to the particle size distribution via a basic model that can readily be applied in an industrial environment for process improvement and optimization.

To model the particle size distribution, the so-called population balance approach can be quite helpful (Randolph and Larson, 1988; Hounslow et al., 1988; Ramkrishna, 2000). The present paper considers a basic population balance model, which was developed to describe the process dynamics of an AkzoNobel fluid bed granulator for a certain chemical species. The aims of the project were to formulate a simple model description of the particle size distribution and to obtain knowledge about how unsteady and unstable behavior of the industrial process can be controlled. The early literature on population balance models focussed on crystallization (e.g. Randolph and Larson, 1988; Sherwin et al., 1969; Lie et al., 1971; Randolph et al., 1973). The present model is quite similar to the so-called mixed reactor mixed product or mixed reactor selective product concepts in older works. However, there are subtle differences in the present model (such as a nonzero nucleation diameter), which leads to a previously unknown nucleation constraint for the existence of a steady state. The application of population balance models to fluid bed spray granulation processes has received some attention in literature before (Heinrich et al., 2002; Drechsler et al., 2005; Radichkov et al., 2006; Peglow et al., 2007). For example, milling of coarse particles and reintroducing the milled material into the granulator was found to produce oscillatory behavior (Heinrich et al., 2002). Compared to the existing models of fluid bed granulation processes, the present model has deliberately been made more simple. The advantage of a simple model is that it is more accessible for mathematical analysis, and in this way important properties of the model can be revealed. It appears that a population model can be stripped down to basic ingredients and nevertheless be able to describe important features of particulate industrial processes.

The contents of the paper is as follows. In section 2 we describe the relevant parts of the industrial process and show available plant data. The population balance model is formulated in section 3. The steady state solution and the corresponding existence condition are derived in section 4, in which the solution of the model is also compared with the plant data. In section 5 we argue that the nucleation parameter in some cases depends on the bed height, and we formulate a corresponding expression for this parameter. Results of numerical simulations are presented in section 6, to show the transient behavior of the model, both for constant and height dependent nucleation. The linear stability of the model is analyzed in section 7. Finally, the conclusions are summarized in section 8.

2. Plant data

In this section relevant information of the granulator is specified and measured particle size distributions are shown. A sketch of the granulator is shown in Fig. 1. The main compartment of the granulator is cylindrical and contains a fluidized bed of height h. The bottom of the bed is cylindrical with area $A = 5\text{m}^2$. The bed is fluidized by a vertical hot air flow (arrows 2 in Fig. 1) through a perforated bottom plate. The superficial air

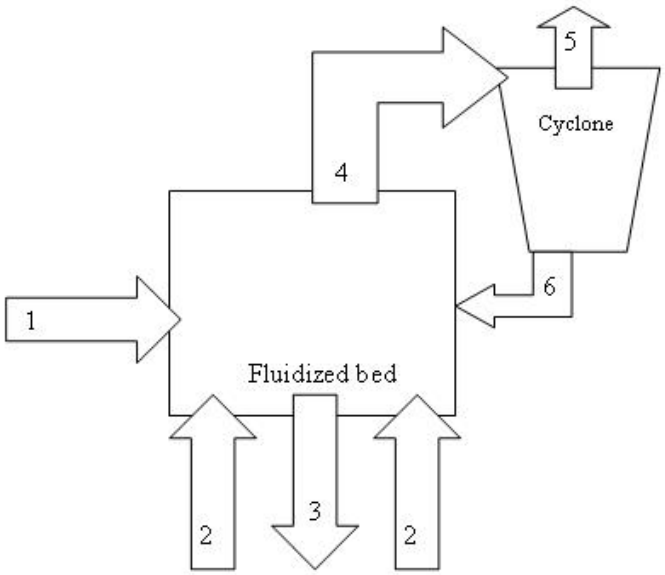

Figure 1: Sketch of the granulator. Arrows: (1) injection of the suspension, (2) injection of hot air, (3) product removal, (4) flow to the cyclone, (5) air outlet, (6) fine particles reentering the bed.

velocity equals 2.5m/s, which is somewhat higher than the minimum fluidization velocity of 1.75m/s. The granulation is a continuous process, as material is removed via a centrally positioned air sifter.

A solution enters at the side of the bed in the form of droplets through various nozzles (arrow 1), spraying in the horizontal direction and positioned at a height of $h_{noz} = 0.44$m above the bottom. In the granulator the water content of the spray droplets quickly evaporates because of the high bed temperature, and the solute is transformed into a new granule (nucleation) or adds to existing granules (growth). The granules are spherical solid particles.

Dividing the spray solute mass flow by the material density of the solid particles, we obtain an effective spray inflow volume flow, Φ, which equals $1.67 \cdot 10^{-4}$ m^3/s. It is emphasized that Φ does not refer to the entire suspension but to the solute content only. The typical hold up of the granulator corresponds to a solids volume of $V = 1.1$m^3. Thus the bed height can be obtained from

$$h = \frac{V}{(1-\epsilon)A}, \tag{1}$$

where ϵ denotes the bed porosity. If the porosity were 0.5, the bed height would be just the nozzle height. It was not possible to measure the actual bed height or porosity, but the operations staff believes that the spray inlets are just below the bed surface. To stimulate particle growth, the spray inlets should not be high above the bed height, while, to avoid particles sticking together, the inlets should not be placed much below the bed surface.

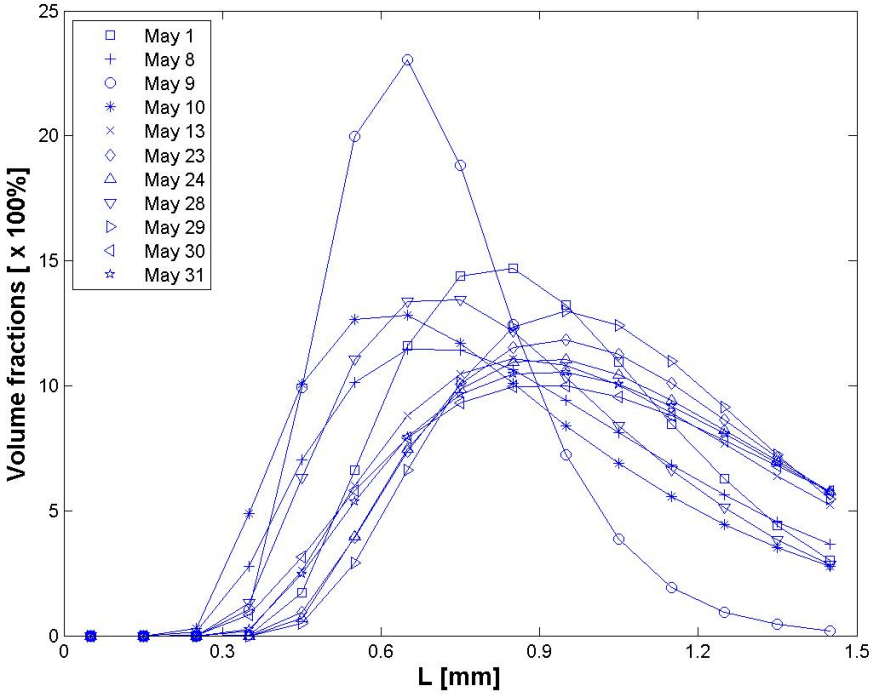

Figure 2: Volume fractions ($\times 100\%$) in the bed as a function of particle size. The samples were taken on May 1, 8, 9, 10, 13, 23, 24, 28, 29, 30, 31 (2008).

The product particles are withdrawn from the center of the granulator (arrow 3). The withdrawal apparatus contains an air sifter with countercurrent flow, to separate small from large particles. The large particles are transported to a storage location, while the small particles are reblown into the fluidized bed to continue granulation.

Because the terminal velocity of the fine particles in the bed is smaller than the superficial air velocity, fine particles flow with the air into the cyclone (arrow 4). The cyclone serves as a recycler for the particles to limit material losses; filtered air escapes through the roof (arrow 5), while the fine particles are brought back to the bed (they are injected below the bed surface, arrow 6).

Particle size distribution measurements taken at the plant are shown in Fig. 2 for the granules in the bed. The figure shows results for samples taken on more or less random days within one month. Each sample from the bed corresponds to one litre of solids, taken out of the bed and subsequently subjected to size analysis by a laser diffraction technique, using particle size classes with a width of 0.100mm each. Since we do not know the start-up times of the runs from which the samples were taken, nor the hour in which they were taken, we can not precisely deduce the history of a single run from the present experimental data. Nevertheless, the variation of the measurements shown in Fig. 2 does indicate that the granulation process is unsteady. Since the residence time of particles in the granulator is about two hours while a run lasts about a week, the different measurements should most probably not be considered as different stages in the

convergence process to a single steady state. The median diameter d_{50} corresponding to the particle size distributions shown in Fig. 2 varies in between 0.68mm and 1.06mm, and equals 0.93mm on average.

3. Population balance model

Let us denote the population density by $n(L,t)$, based on the total number of particles in the bed. The population density is a function of particle diameter (L) and time (t). We assume spatial homogoneity of the population in the bed. The amount $n\ dL$ denotes the number of particles within the size class $[L, L+dL]$.

A quite general formulation of the population balance equation reads (Randolph and Larson, 1988; Hounslow et al., 1988):

$$\frac{\partial n}{\partial t} + \frac{\partial (Gn)}{\partial L} = B - Dn + O, \tag{2}$$

Here G denotes the growth rate of particles. The first term on the right-hand side is the birth-term B, which is a source-term representing the particles created by nucleation. The second term is the death-term Dn, which denotes the removal of product particles from the bed to the silo. Finally, there is a term O,which represents other effects, such as aggregation, attrition and interaction with the cyclone. In the following we further specify the models for G, B, D and O.

The growth of the particles is primarily due to the spraying of solution upon existing particles. Because of the high bed temperature, fast drying of the spray is assumed, such that temperature, saturation state and humidity do not appear in the system of equations. We model the total volume that is added to existing particles in a time span dt by $(1-b)\Phi dt$, where $1-b$ is a fraction between 0 and 1, and Φ the effective spray inflow volume flow specified in the previous section. On the one hand, it is reasonable to assume that the amount of spray captured by a particle of size L in a time span dt is proportional to its surface (πL^2). On the other hand the increase of volume of the particle is equal to the volume of the deposited layer on the particle's surface, $\pi L^2(\frac{1}{2}Gdt)$, which is also proportional to L^2. Therefore, the growth-rate G does not depend on L (the McCabe law, see Randolph and Larson (1988)). The total volume of the new layers equals

$$\tfrac{1}{2}Gdt\pi \int_0^\infty nL^2 dL. \tag{3}$$

Note that G is the growth-rate of the diameter; the growth-rate of the radius equals $\frac{1}{2}G$. Equating the volume of the new layers with $(1-b)\Phi$, results in an equation for the growth-rate,

$$G = \frac{2(1-b)\Phi}{\pi \int_0^\infty nL^2 dL}, \tag{4}$$

which is a function of time.

Some spray droplets dry entirely before they hit any other particle in the bed. These droplets do not contribute to growth, but to nucleation. With nucleation we mean the process of formation of the smallest particles present in the bed. Denoting the spray

fraction from which particles are nucleated with b, we have a nucleation volume flux of $b\Phi$. The simplest model for nucleation invokes a delta-function centered around the minimum particle diameter L_0,

$$B = \frac{b\Phi}{\frac{1}{6}\pi L_0^3}\delta(L - L_0), \tag{5}$$

Note that the volume integral $\int_0^\infty \frac{1}{6}\pi L^3 B dL$ equals $b\Phi$ (the dimension of the δ-function is m^{-1}).

The simplest way to model product withdrawal (the death-function D) is to use an Heaviside function around the sifting diameter L_1 multiplied with a constant s (the product withdrawal rate)

$$D = sH(L - L_1), \tag{6}$$

such that D equals zero for $L < L_1$ and s for $L > L_1$. The parameter s denotes which fraction of the particles of size L withdrawn from the bed during a second, provided $L > L_1$. The average particle residence time equals $1/s$ in case the sifter is switched off ($L_1 = L_0$).

The last term, O, is put to zero, by which we either ignore attrition and aggregation, or assume them to be lumped into the growth-term (see for example Heinrich et al. (2002), where a surface-based attrition model similar to the growth term was used). The net effect of the cyclone is also ignored (we assume that the solids flux to and from the cyclone are equal, which also implies no loss of material in the cyclone).

In summary, our basic model reads:

$$\frac{\partial n}{\partial t} + G\frac{\partial n}{\partial L} = \frac{b\Phi\delta(L - L_0)}{\frac{1}{6}\pi L_0^3} - sH(L - L_1)n, \tag{7}$$

$$G = \frac{2(1-b)\Phi}{\pi \int_0^\infty nL^2 dL}, \tag{8}$$

with $0 < L_0 \leq L_1$, $0 \leq b \leq 1$, $\Phi > 0$, $s > 0$, boundary condition $n(0,t) = 0$ and initial condition $n(L,0) = 0$.

4. Steady state derivation

In the steady state $\partial n/\partial t = 0$ and G is a constant. The fact that the value of G is not a free parameter, but depends on a property of n makes the analytical solution of this equation interesting. In the steady state equation (7) reduces to

$$G\frac{dn}{dL} = B - Dn. \tag{9}$$

This is a first-order linear differential equation, which can be solved analytically using the method of variation of constants:

$$n(L) = c(L)\exp[-\int_0^L \frac{D(L')}{G}dL'], \tag{10}$$

$$c(L) = \int_0^L \frac{B(L')}{G}\exp[\int_0^{L'} \frac{D(L'')}{G}dL'']dL'. \tag{11}$$

After substitution of the expressions for B and D we obtain,

$$n(L) = \begin{cases} 0 \quad \text{if} \quad L < L_0 \\ \frac{b\Phi}{\frac{1}{6}\pi L_0^3 G} \quad \text{if} \quad L_0 < L < L_1 \\ \frac{b\Phi}{\frac{1}{6}\pi L_0^3 G} \exp[-s(L-L_1)/G] \quad \text{if} \quad L > L_1. \end{cases} \tag{12}$$

The solution presented in equation (12) expresses that the steady-state particle size distribution equals zero up to the nucleation diameter L_0, attains a constant value between L_0 and sifting diameter L_1, and drops exponentially for diameters larger than L_1.

The steady state solution is not complete yet; we still have to find the corresponding growth-rate G. Substitution of $n(L)$ in the growth-rate definition (8) and performance of several partial integrations yield:

$$G = \frac{2(1-b)\Phi}{\pi \frac{b\Phi}{\frac{1}{6}\pi L_0^3 G}\left(\frac{1}{3}(L_1^3 - L_0^3) + \frac{GL_1^2}{s} + 2\frac{G^2 L_1}{s^2} + 2\frac{G^3}{s^3}\right)}. \tag{13}$$

This is equivalent to

$$\frac{6bL_1^3}{L_0^3}\left(\frac{1}{3}(1 - \frac{L_0^3}{L_1^3}) + \frac{G}{sL_1} + 2\frac{G^2}{s^2 L_1^2} + 2\frac{G^3}{s^3 L_1^3}\right) = 2(1-b), \tag{14}$$

which can be rewritten as the constraint

$$6q^3 + 6q^2 + 3q = p \tag{15}$$

with q and p defined as

$$q = \frac{G}{sL_1}, \tag{16}$$

$$p = \frac{(L_0/L_1)^3}{b} - 1. \tag{17}$$

Since by definition q must be positive, the polynomial has a physical solution for positive p only. Thus a steady population of the bed exists only if

$$b \leq \left(\frac{L_0}{L_1}\right)^3, \tag{18}$$

equivalent to $b \leq r^3$, using the definition

$$r = L_0/L_1. \tag{19}$$

When condition (18) is fulfilled, the steady-state growth rate G is given by the single positive root of (15), which can approximately be obtained from the q-value in Fig. 3, for given p. According to the polynomial (15) the steady-state growth-rate does not depend on the spray flow rate Φ, which is another interesting conclusion that can be drawn from this analysis.

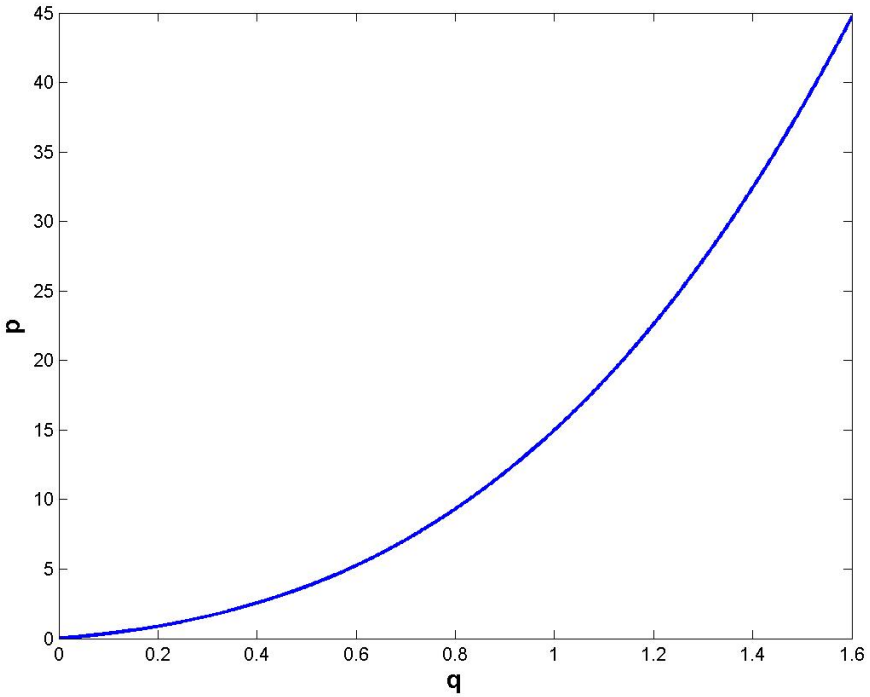

Figure 3: Growth-rate equation (15): p against q.

Inequality (18) implies that the amount of nuclei created (b) should be sufficiently small, otherwise a steady state does not exist. The condition can also be interpreted in terms of particle numbers. Let us denote the coefficient in front of the delta-function in (7) by B_0. Hence $B_0 = b\Phi/\frac{1}{6}\pi L_0^3$ and represents the number of particles nucleated per second. The steady-state condition (18) is equivalent to

$$B_0 \leq \frac{\Phi}{\frac{1}{6}\pi L_1^3}. \tag{20}$$

This condition is independent of the nucleation diameter L_0 and expresses that the number of new solid particles (created per time unit) should be smaller than the volumetric spray flux Φ divided by the volume of a particle at the minimum withdrawal diameter L_1.

The hold-up or the total volume of the solids in the bed (V) is defined by

$$V = \tfrac{1}{6}\pi \int_0^\infty nL^3 dL. \tag{21}$$

If we substitute the analytical solution (12) into this expression we obtain the bed volume in the steady state:

$$V = \frac{\Phi}{s}\Big(1 + \frac{b(1-r^4)}{4r^3 q}\Big). \tag{22}$$

The case $L_1 = L_0$ (equivalent to $r = 1$) corresponds to uniform product withdrawal. In that case the sifter has no effect; the lowest particle size in the product is the nucleus

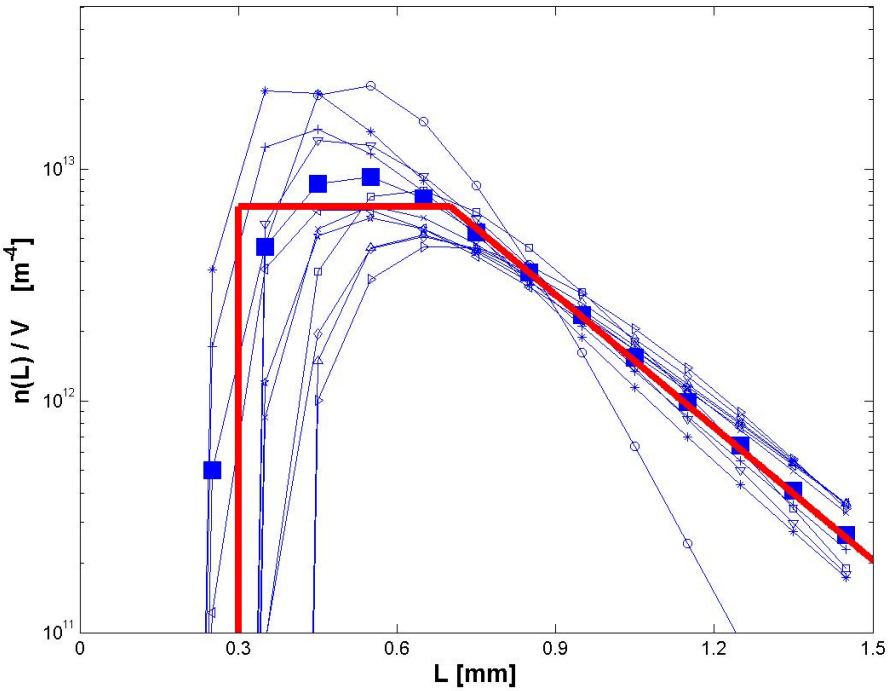

Figure 4: Number density functions for the particles in the bed (scaled with the bed volume); non-averaged plant data (small symbols, dates left out for space in the figure) and averaged plant data (large symbols) compared to the model predictions $n(L)$ for $b = 0.028$ (solid line, no symbols).

size. Then V simply equals Φ/s. If we divide equation (22) by Φ, we obtain V/Φ, which is the average particle residence time (larger than or equal to $1/s$).

In order to compare with the available plant data, it is convenient to derive a volume density function $v(L)$ from the number density function n by the definition

$$v(L) = \frac{\frac{1}{6}\pi n\ L^3}{V} = \frac{f(L)L^3/L_1^4}{qr^3/b + (1-r^4)/4}, \tag{23}$$

where $f(L)$ equals 0 for $L < L_0$, 1 for $L_0 < L < L_1$, and $\exp[(1 - L/L_1)/q]$ for $L > L_1$. Because of the normalization with V the integral of $v(L)$ over all L equals 1. From the measured volume percents shown in Fig. 2, a volume density function can be obtained by dividing the volume percents by ΔL and by 100%, where ΔL=0.1mm is the width of a single measured particle size interval. Subsequently, using equation (23), the measured number density function $n(L)$ can be derived from the measured bed functions $v(L)$. The measured number density functions are shown in Fig. 4 (symbols). According to this figure, a particle size distribution is roughly characterized by a minimum particle size, a more or less flat region, and a region of exponential decay.

Equation (23) shows that $v(L)$, and also $n(L)/V$, are independent of Φ and s. Since q is a function of b, L_0 and L_1, the nucleation parameter and the length-scales are the only parameters that determine $v(L)$ and $n(L)/V$. The hold-up volume V does depend on Φ and s, that is on their ratio. In the steady state, the function v contains a maximum at

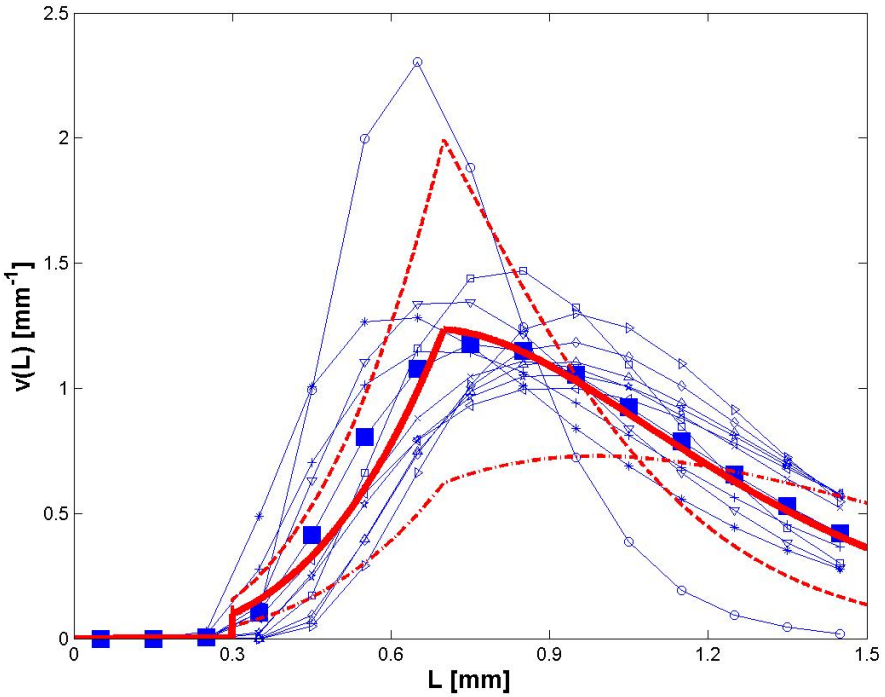

Figure 5: Volume density functions for the bed; non-averaged plant data (small symbols, dates left out for the clarity of the figure) and averaged plant data (large symbols) compared to the model predictions $v(L)$ for three different values of b (no symbols): 0.018 (dash-dotted), 0.028 (solid), and 0.038 (dashed).

the particle diameter L_m, which is given by

$$L_m = \max(L_1, \frac{3G}{s}). \tag{24}$$

Note that $L_m > L_1$ is equivalent to $q > \frac{1}{3}$.

Next we show how the available plant data can be used to estimate the model parameters. The flux Φ equals $1.67 \cdot 10^{-4}$m^3/s. To approximate the average of the measured number densities (the average is also shown in Fig. 4) by a function of the form (12), L_0=0.3mm and L_1=0.7mm appear to be appropriate estimates. Since the vertical axis in Fig. 4 is logarithmic, the straight slope of the tail denotes an exponential decay. Thus the tail of the analytical solution matches the experimental average if the analytical exponential coefficient,

$$-s/G = -1/(qL_1), \tag{25}$$

equals -4400, which is the slope of the tail in Fig. 4 multiplied with ln(10). Since L_1=0.7mm, the value $q = 0.325$ is now obtained, which implies $b = 0.028$. This means that 2.8% of the solute content of the spray generates new nuclei and 97.2% is used for particle growth. It is remarked that b is smaller than $r^3 = 0.078$, which is required for the existence of a steady-state. Since the total bed volume should equal about 1.10m^3, equation (22) leads to the withdrawal rate $s = 1.92 \cdot 10^{-4}$/s. This means that the probability of a particle of size $L > L_1$ to be withdrawn from the bed in a given second equals about 0.0002. Finally $G = 4.37 \cdot 10^{-8}$m/s follows from equation (25). This means that the particle diameter grows 0.157mm per hour.

Table 1: Steady state predictions for G, V and d_{50} for different values of b ($L_0 = 0.3$mm, $L_1 = 0.7$mm, $s = 1.92 \cdot 10^{-4}\text{s}^{-1}$ and $\Phi = 1.67 \cdot 10^{-4}\text{m}^3/\text{s}$).

b [$\times 10^{-3}$]	G [$\times 10^{-8}$ m/s]	V [m^3]	d_{50} [mm]
0.018	6.33	0.97	1.265
0.028	4.37	1.10	0.952
0.038	3.08	1.31	0.790

The comparison between measured and modelled $v(L)$ is shown in Fig. 5. For the values of the parameters mentioned above, the simple model appears to be able to describe the shape of the experimental average distribution curve for v (and n) and the experimental bed hold-up reasonably well. Fig. 5 and Table 1 contain model predictions for three different values of b, and thereby demonstrate how the steady state changes with b, provided L_0, L_1 and s remain constant. Table 1 shows that the growth rate and the median particle diameter (d_{50}) both increase with increasing generation of nuclei (b). According to the table a lower median diameter corresponds to a larger bed volume. This is logical, because the sifter prevents small particles to be withdrawn from the bed. The variations for different b show that each experimental sample may be regarded as a quasi-steady state, which is justified if b varies slowly compared to the transient dynamics of equation (7).

For plant operation it is not only interesting to know the steady state of the model, but also to investigate the transient behavior towards the steady state and the stability of the steady state. The latter two issues are subjects of the next sections.

5. Volume dependent nucleation

Sofar a simple population balance model for a fluid bed granulator has been presented. The steady-state solution has analytically been determined, and it has been proven that a steady state solution does not exist in case the nucleation parameter exceeds a certain threshold. The analytical steady-state solution has also been compared with experimental data from a plant.

In the present and following sections we consider the behavior of the particle size distribution and derived properties as functions of time, by means of numerical simulation. First the model is refined, by modelling the nucleation parameter as a function of the depth of the bed, i.e. the total volume of particles in the fluid bed. Then the stability of the solution is examined numerically and analytically, and it appears that in some cases the solution displays non-decaying oscillations around the theoretical steady state.

A relation between b and h should at least globally respect the physical behavior of the nucleation parameter b. This means that b should decrease if the voidage at the height of the spray nozzles decreases, since a lower voidage implies that a droplet has less time to dry until the first collision with a bed particle takes place and therefore has a smaller chance to become a nucleus. A standard picture of a fluidized bed is that below the bed height (the fill level of the bed) the voidage is approximately constant, while above the bed height the voidage rapidly increases with height (Kunni and Levenspiel,

1987). Consider now a granulator that is gradually filled from empty to full; hence the bed height h gradually increases. When the granulator is still empty ($h = 0$) the fraction b should be one, since there are no particles available for growth yet. Then a period starts in which the bed height increases but still remains below the nozzle height h_{noz}=0.44m. In this regime ($0 < h < h_{noz}$) the spray is injected into the elutriation zone above the bed. Since some spray droplets will be captured by elutriated particles b should be smaller than one. While the bed height is rising to the nozzle height, the volume fraction of granules at the nozzle height increases. Thus b should decrease with h in the regime $h < h_{noz}$. When h has reached h_{noz}, the granulator may be filled further, and then another regime is entered (bed height $h > h_{noz}$). Since in this regime the spray nozzles are fully immersed in the bed, the voidage at the nozzle height remains more or less constant when h rises further. Hence b is approximated with a constant (b_∞) in the regime $h > h_{noz}$. We take $b_\infty = 0.028$, the empirical value from the previous section. The behavior of b as function of h that has just been described is shown in Fig. 6a, which corresponds to the function

$$b(h) = b_\infty + \max\Big(0, (1 - b_\infty)\frac{h_{noz} - h}{h_{noz}}\Big). \tag{26}$$

We argued above that b should decrease monotonically for $h < h_{noz}$, but apart from this the functional relationship $b(h)$ is not known in this regime. We therefore took the simplest approximation possible, which is a first order (linear) interpolation in the region $0 < h < h_{noz}$. Note that the linear stability results that will be presented later on (section 7) are not restricted to equation (26). For linear stability not the entire function $b(h)$, but only the local value of the slope ($\partial b/\partial h$) is important. In section 7 various levels of $\partial b/\partial h$ will be considered.

The fluid bed height h can be approximated by (Kunni and Levenspiel, 1987)

$$h = \frac{V}{(1 - \epsilon)A}, \tag{27}$$

which is proportional to the total particle volume. In this work we use a value of 0.5 for the fluid bed voidage ϵ, which is slightly higher than the minimum fluidization voidage (Kunii and Levenspiel, 1987). Because of equation (27), the function b essentially depends on the total particle volume V, which is the third moment of the number density n. This adds another nonlinearity to the basic population balance equation; in addition to the second moment of n, which occurs through the growth-rate definition, the third moment of n appears into the equation, through dependence of b on V.

We consider four different cases (Table 2), corresponding to variations of important control parameters in the actual industrial process. Compared to the standard case (C0), the spray mass flux is reduced in case C1 and C2 to 90% and 80% respectively. In case C3 the sifter is switched off; the product withdrawal is not selective in case C3 ($L_1 = L_0$).

Because of the relation between bed height and total volume (equation (27)), the steady state relation between b and V (equation (22)) can be written as a function $b_i(h)$, for each case Ci listed in Table 2. The curves $b_i(h)$ have been drawn on a zoom of Fig. 6a, resulting in Fig. 6b. To plot $b_i(h)$ we parametrized the coordinates (b, h) of the curve

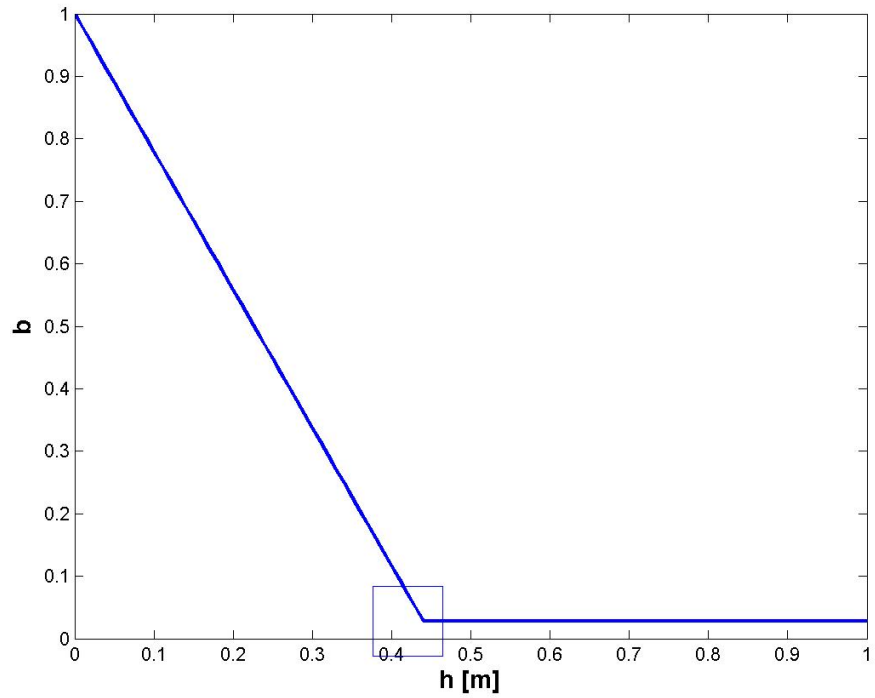

(a)

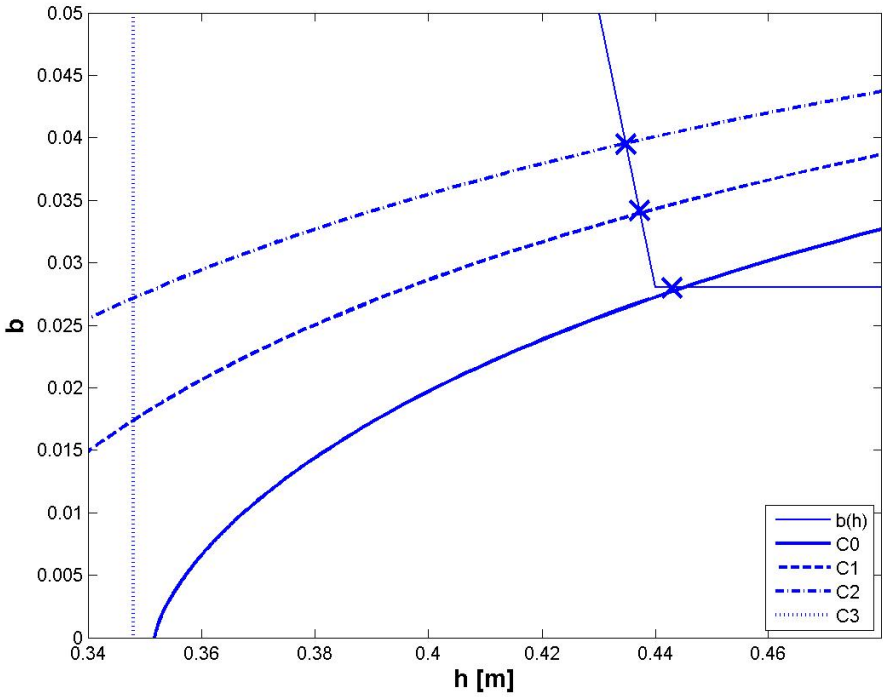

(b)

Figure 6: Nucleation fraction parametrization $b(h)$ ((a) and thin solid curve in (b)). Fig. (b) zooms in on the essential part indicated by the window in (a). Fig. (b) also shows the curves $b_i(h)$ representing equation (22) for each case: C0 (base case; thick solid), C1 (90% flux; thick dashed), C2 (80% flux; thick dash-dotted) and C3 (no sifter; thick dotted). The crosses denote steady state points.

Table 2: Different cases using the nucleation function $b(h)$ with $b_\infty = 0.028$ and $h_{noz} = 0.44$m. A reference spray flux Φ_0 is defined; $\Phi_0 = 1.67 \cdot 10^{-4}\mathrm{m}^3/\mathrm{s}$.

Case	Φ/Φ_0	L_0 [mm]	L_1 [mm]	s [10^{-4}/s]
C0	1	0.3	0.7	1.92
C1	0.9	0.3	0.7	1.92
C2	0.8	0.3	0.7	1.92
C3	1	0.3	0.3	1.92

by ($q > 0$):

$$b_i = \frac{r^3}{6q^3 + 6q^2 + 3q + 1}, \tag{28}$$

$$h = \frac{\Phi}{s(1-\epsilon)A}\Big(1 + \frac{1 - r^4}{4q(6q^3 + 6q^2 + 3q + 1)}\Big). \tag{29}$$

Equation (28) follows from equations (15) and (17), and equation (29) from equations (27), (22) and subsequent substitution of (28).

For each case i, the intercept of the curve $b_i(h)$ with the curve $b(h)$ given by Eq. (26) defines the steady state point (b, h), denoted with a cross in Fig. 6b. Note that the intercept of case C3 is not shown in Fig. 6b, because the corresponding value of $b = 0.23$ falls outside the zoom region. Only in the standard case C0 the steady state point is located at the horizontal tail of the curve $b(h)$.

In the next sections, where the dynamic behavior of the different cases is studied numerically and analytically, it becomes clear that the local slope of the $b(h)$ curve is important for the stability of the steady state point. If the slope at the steady state point is horizontal the system is stable (C0). By decreasing the flux Φ, the steady state point moves to the region with negative slope, where the system is unstable (if the sifter is switched on). This is consistent with the experience of the operation staff at the plant that an increase of the flux leads to a more robust process.

6. Transient numerical simulations

In this section we present numerical solutions of the time-dependent system of equations. The system is specified by the partial differential equation (7) equipped with the function definitions (8), (26), (27) and (21). A four-stage Runge Kutta method for the time integration (with time step of 0.5s) and the standard first-order upwind method for the spatial discretization are employed. The spatial mesh contains 1000 points in the computational domain $0 < L < 10$mm, with a constant grid spacing of 0.05mm up to L=2.5mm, while for larger L the intervals increased using a relative factor of 1.002 between adjacent intervals. The boundary condition prescribes $n(0) = 0$, while for the initial condition the analytical steady state solution is used for an approximate initial value of G.

Simulation results for the four cases listed in Table 2 are shown in Fig. 7 (the bed height h and growth G). Apparently the steady state solution is stable in cases C0 and

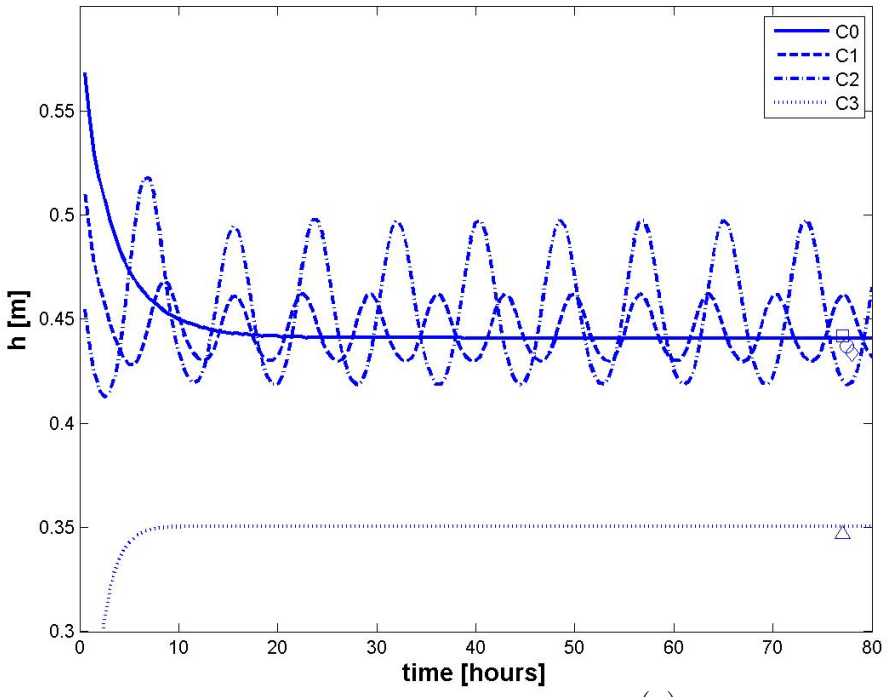

(a)

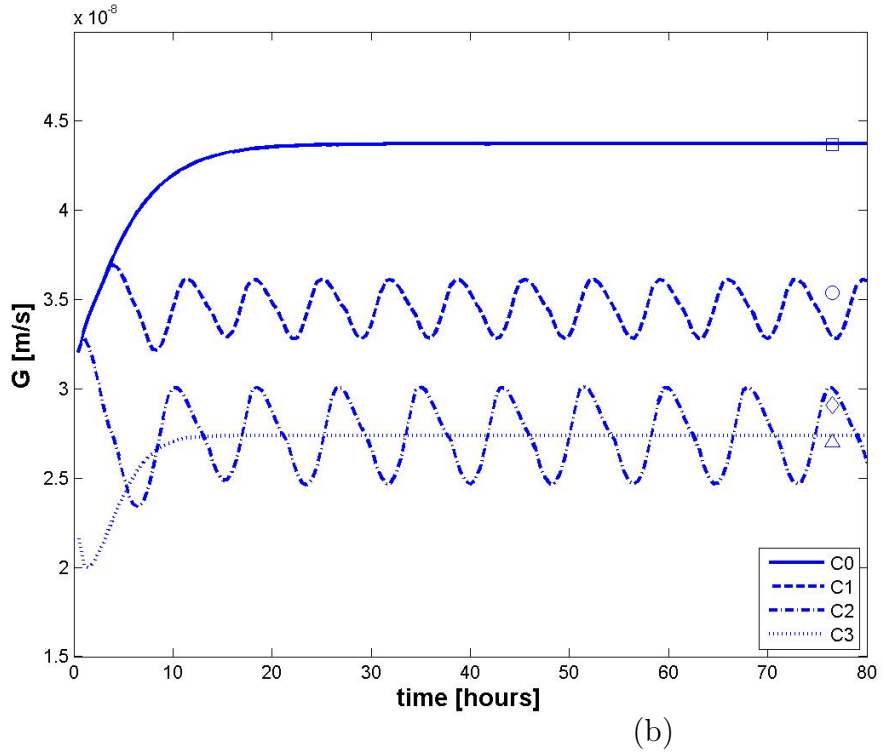

(b)

Figure 7: Transient results from the numerical simulations: bed height (a) and particle growth rate (b). The curves correspond to the cases listed in Table 2: C0 (base case; solid), C1 (90% flux; dashed), C2 (80% flux; dash-dotted) and C3 (no sifter; dotted). The symbols denote the analytical steady-state values: C0 (circle), C1 (square), C2 (diamond), C3 (triangle).

C3, but unstable in cases C1 and C2. The unstable cases correspond to a lower spray flux. Comparing cases C1 and C2 with C0 in Fig. 6, it appears that the stable case corresponds to a steady state on the horizontal part of $b(h)$, the spray is injected just below the bed surface. However, the unstable steady states lie on the decaying part of $b(h)$. In the unstable cases, the steady-state bed height is lower than h_{noz}; the spray enters the granulator above the bed surface.

Comparing case C3 with C0, it appears that in case the sifter is switched off (C3), the steady state is stable even though the spray is injected above the bed surface. Apparently, the selective product withdrawal is essential to let the instability occur. Both the period and the amplitude of the oscillations are found to increase with decreasing spray flux (compare case C2 to case C1).

The results have been validated by grid refinement in space and time; there would be no visual difference between the fine grid curves and the present curves if the fine grid curves were added to the figures. Also the values for the corresponding analytical steady state solutions were plotted on Fig. 7. In the stable cases the numerical and analytical steady states nearly coincide; compare for example the steady state value of G for case C0 in Fig. 7b with the analytical value (circle, representing the value $4.37 \cdot 10^{-8}$m/s from Table 1).

7. Linear stability

In this section a linear stability analysis is performed to investigate the unstable behavior around the steady state. Since a linear stability analysis is valid for small perturbations only, it is primarily relevant for the onset of the instability. One result of the analysis is that stability is only ensured provided the absolute slope of the semi-monotonically decreasing $b(h)$-curve is less than a critical value.

Linear stability analysis is a frequently used tool to investigate population balance models. For crystallization models (where nucleation in the fluid was modelled in terms of supersaturation) linear stability analyses have been performed for stepwise expressions of the death-term in the population balance equation (Sherwin et al., 1969; Lei et al., 1971; Randolph et al., 1973; Randolph and Larson, 1988). The stability of fluid bed spray granulators has been investigated with use of numerical nonlinear stability techniques (Radichkov et al. 2006), but as far as we know, a linear stability analysis of a population balance equation for a fluid bed spray granulator has not been performed before. A straightforward application of the methods of moments is quite inconvenient in the present case, since the sifter partial moments (corresponding to a part of the diameter range) are involved. Thus the number of moments doubles and results in a determinant of a dense matrix of 8×8, which is inconvenient to handle. We therefore adopt an alternative approach which results in a determinant of a 2×2 matrix only.

A linear stability analysis of a steady state is only meaningful if the steady-state exists, so we can now nondimensionalize the equations with the steady state growth-rate $\overline{G}$ and the length-scale L_1, using,

$$\tilde{n} = L_1 n, \quad \xi = L/L_1, \quad \tau = t\overline{G}/L_1, \quad \sigma = sL_1/\overline{G}, \quad r = L_0/L_1, \quad \phi = \Phi/L_1^2\overline{G}.$$

The growth-rate $\overline{G}$ corresponds to the steady state value of the nucleation parameter, $\overline{b}$, such that constraint (15) is satisfied. In addition we introduce the parameter β proportional to the derivative of b:

$$\beta = \frac{\phi L_1^3}{(1-\overline{b})r^3}\ \frac{\partial b}{\partial V} = \frac{\phi L_1^3}{(1-\overline{b})r^3(1-\epsilon)A}\ \frac{\partial b}{\partial h}. \tag{30}$$

It represents the scaled slope of the function $b(h)$, for example $b(h)$ shown in Fig. 6. The derivative $\partial b/\partial h$ is evaluated at the steady state point corresponding to $\overline{b}$. One important value of β is zero. Then b does not depend on h (as for example on the horizontal tail of the function $b(h)$ in Fig. 6, when the spray nozzles are immersed). In addition, we are interested in cases with $\beta < 0$, to analyze the stability of the system if b is decreasing with increasing bed height (as for example on the decaying part of the function $b(h)$ in Fig. 6, when elutriated particles catch droplets).

The linear stability analysis is based on the following decomposition of the nondimensional number density $\tilde{n}$:

$$\tilde{n} = \overline{n} + \mathrm{Re}(n'(\xi)e^{z\tau}), \tag{31}$$

where $\overline{n}$ represents the nondimensional steady state and $n'(\xi)$ a complex nondimensional fluctuation profile propagating with the complex nondimensional eigenvalue z. Stability occurs if $\mathrm{Re}(z) \leq 0$. Next we substitute the equation above in the population balance equation and linearize by omitting terms of order two in n' (or higher). The result takes the form:

$$\Big(c_1 \cos(\mathrm{Im}(z)\tau) + c_2 \sin(\mathrm{Im}(z)\tau)\Big)\ \exp(\mathrm{Re}(z)\tau) = 0, \tag{32}$$

where c_1 and c_2 are real coefficients independent of τ. For equation (32) to be valid for all times, the coefficient c_1 should be zero, which leads to the real part of the following equation, and coefficient c_2 should also be zero (if $\mathrm{Im}(z) \neq 0$), which leads to the complex part of the following equation:

$$\begin{aligned} \frac{dn'}{d\xi} &= -zn' - H(\xi-1)\sigma n' + (1-\overline{b})\beta m_3' \tilde{\delta}(\xi - r) + \\ &\quad \Big(\frac{\frac{1}{3}r^3(1-\overline{b})\beta m_3'}{\overline{m}_2} + \frac{m_2'}{\overline{m}_2}\Big)\frac{d\overline{n}}{d\xi}. \end{aligned} \tag{33}$$

Here $\tilde{\delta} = L_1\delta$ is the nondimensional δ-function; the integral of $\tilde{\delta}$ over ξ-space equals one. Equation (33) expresses an eigenvalue problem with the eigenfunction n' and eigenvalue z. The equation contains symbols that refer to specific moments:

$$m_2' = \int_0^\infty \xi^2 n' d\xi, \quad m_3' = \int_0^\infty \xi^3 n' d\xi, \tag{34}$$

and

$$\overline{m}_2 = \int_0^\infty \xi^2 \overline{n} d\xi = \frac{2\phi(1-\overline{b})}{\pi}. \tag{35}$$

Since the steady state is known,

$$\overline{n} = \frac{\overline{b}\phi}{\frac{1}{6}\pi r^3} H(\xi - r)\ \min(1, e^{-\sigma(\xi-1)}), \tag{36}$$

the eigenfunction n' can be solved from equation (33) using the variation of constants. This results in $n'(\xi) = 0$ for $\xi < r$,

$$n'(\xi) = (\gamma m_2' + \beta m_3')e^{-z(\xi - r)}, \tag{37}$$

for $r \leq \xi \leq 1$, and

$$\begin{aligned} n'(\xi) &= (\gamma m_2' + \beta m_3')e^{-(z+\sigma)(\xi-1)-z(1-r)} + \\ &\quad (\gamma m_2' + \bar{b}\beta m_3')\frac{\sigma}{z}\Big(e^{-(z+\sigma)(\xi-1)} - e^{-\sigma(\xi-1)}\Big) \end{aligned} \tag{38}$$

for $\xi > 1$. The constant γ is defined by

$$\gamma = \frac{3\bar{b}}{(1-\bar{b})r^3}. \tag{39}$$

The solution n' should satisfy the two constraints expressed by (34) which leads to the following system

$$a_1 m_2' + a_2 m_3' = 0, \tag{40}$$

$$a_3 m_2' + a_4 m_3' = 0, \tag{41}$$

which has a nontrivial solution only if the determinant f equals zero,

$$f(z) = a_1 a_4 - a_2 a_3 = 0 \tag{42}$$

The four coefficients a_1 to a_4 are specified in the Appendix.

The expression $f(z) = 0$ is the characteristic equation for the eigenvalue z. It is more complicated than a polynomial, because it contains exponents in z, and this often results in an infinite number of complex roots. The root with the maximum value of $\mathrm{Re}(z)$ determines whether the system is unstable or not. For given parameters the roots of the characteristic equation can be obtained by searching for values z for which $|f| = 0$, for example by drawing a contour plot of the function $|f|$ in the z-plane, using complex arithmetics in Fortran or Matlab.

Figure 8 shows the eigenvalues with an imaginary part $|\mathrm{Im}(z)| \leq 40$ for two values of β: $\beta = 0$ and $\beta = -30$. The steady state considered is the solution of case C0 in the previous section: $\sigma = 3.1$, $r = 0.43$, $\epsilon = 0.5$, $A = 5\mathrm{m}^2$, $L_1 = 0.7\mathrm{mm}$, and $\phi = 7.8 \cdot 10^9$ (note that ϕ only appears through β). The value $\beta = 0$ corresponds to constant b (for example the horizontal part of Fig. 6), while substitution of the slope of the decaying part of the $b(h)$ curve shown in Fig. 6 ($\partial b/\partial h = -2.2/\mathrm{m}$) into the definition of β (30) provides $\beta = -30$ for the parameters of case C0. For $\beta = 0$ (in this case the nozzles are immersed in the bed) all eigenvalues are stable ($\mathrm{Re}(z) < 0$ in Fig. 8a); for constant b the system is stable. However, for $\beta = -30$, which would be applicable if the bed were lower than the nozzle height, all eigenvalues are unstable (for each eigenvalue $\mathrm{Re}(z) > 0$, see Fig. 8b). This means that the steady state of case C0 would be unstable if $\partial b/\partial h$ attained the value of the negative slope in Fig. 6.

The pair of unstable eigenvalues in Fig. 8b has imaginary parts ± 6.0, corresponding to a dimensional period of 4.7 hours. The imaginary part of the eigenvalue is a nondimensional frequency of the linearized model; the frequency of the full nonlinear model

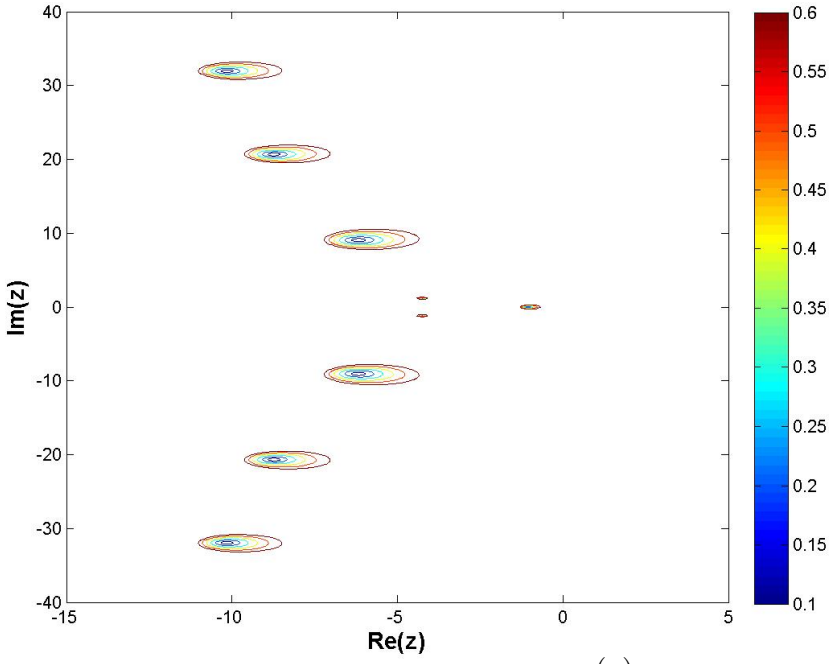

(a)

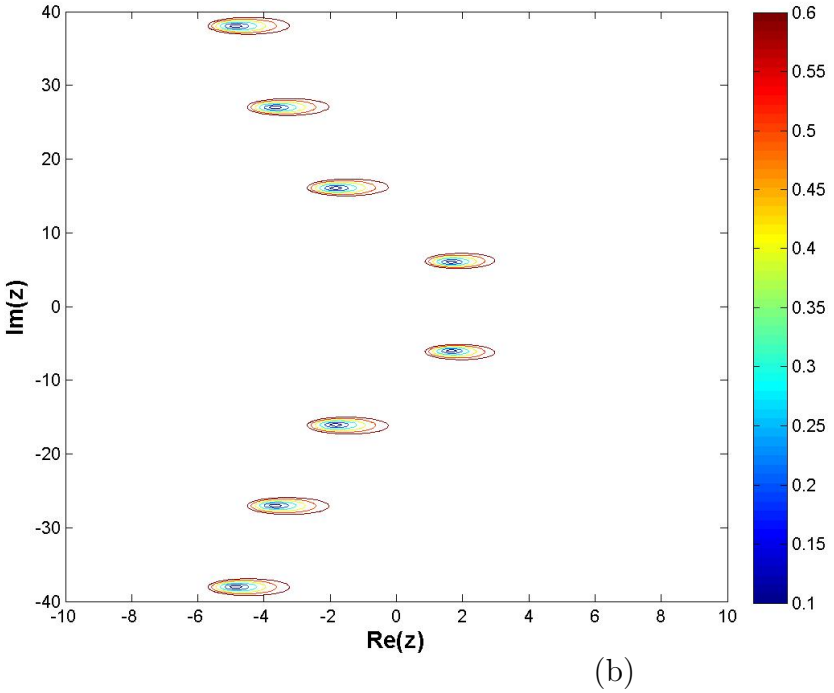

(b)

Figure 8: Low-level contours of the function $|f|$ (contourlevels 0.1, 0.2, 0.3, 0.4, 0.5, 0.6). The distinct spots represent the eigenvalues in the complex plane for a stable case $\beta = 0$ (a) and for an unstable case $\beta = -30$ (b).

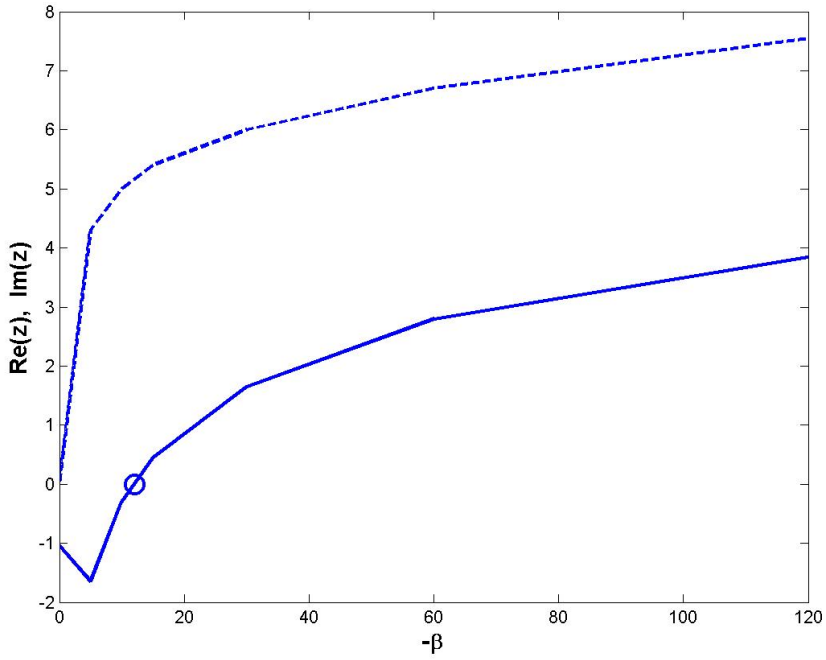

Figure 9: The most unstable eigenvalue z as a function of $-\beta$: Re(z) (solid) and Im(z) for the case $r = 0.43$ and $\sigma = 3.1$. The critical point is denoted with a circle; the system is unstable at the right of the critical point.

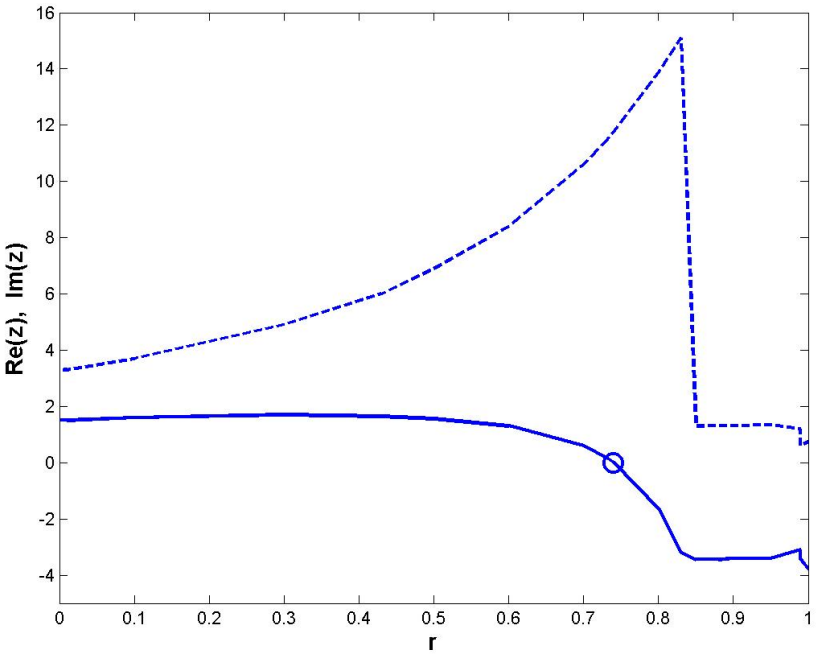

Figure 10: The most unstable eigenvalue z as a function of r; Re(z) (solid) and Im(z) for the case $\beta = -30$ and $\sigma = 3.1$. The critical point is denoted with a circle; the system is unstable at the left of the critical point.

will be about the same, provided the amplitude of the oscillation is small and β remains approximately constant. In this case higher order nonlinear effects lead to a somewhat larger period: the actual period in Fig. 7 is about 6 hours in case C1 and about 8 hours in case C2. It is remarked that for larger $|\beta|$, ($\beta = -120$) another pair of eigenvalues is also unstable, while, most probably, for $\beta \to -\infty$ an infinite number of eigenvalues is unstable. Thus for sufficiently steep slopes, the transient system behavior may show interactions of multiple oscillatory waves with different frequencies.

We finally investigate how the stability depends upon β and r. In between $\beta = -30$ and $\beta = 0$, a critical point occurs (a point where the real part of the largest eigenvalue is precisely zero. The real and imaginary part of the most unstable eigenvalue as functions of $-\beta$ are shown in Fig. 9. According to this figure the critical value of β turns out to be $\beta_{crit} = -12$ for $r = 0.43$ and $\sigma = 3.1$. This means that the system is stable if the descent of the $b(h)$ curve is less steep than 40% of the descending slope shown in Fig. 6. There is also a critical value of r; according to Fig. 10 instability occurs for $r < 0.74$ if $\beta = -30$ and $\sigma = 3.1$. The physical interpretation of the two critical points is as follows: the steady state particle size distribution becomes unstable if the length-scale ratio r is sufficiently large (i.e. if the minimum particle diameter allowed by the sifter is sufficiently larger than the nucleus size) and the dependence of b on h is sufficiently strong (which is most likely the case if the bed surface level is near the height of the spray nozzles).

8. Conclusions

The population balance method is useful to understand and control a wide range of industrial problems. In this paper a simple population balance model was formulated for a fluid bed granulator used by AkzoNobel. The model contains a limited number of parameters: the spray flux Φ, the withdrawal rate s, the minimum product withdrawal length-scale L_1 and two parameters that control the formation of the smallest particles present in the bed (nucleation): the minimum particle size (L_0) and the flux fraction used to form these particles (b, also called the nucleation fraction). The steady state solution for the particle diameter distribution was determined analytically, and it was proven that a steady state solution does not exist if b exceeds a threshold. The analytical steady state solution was favorably compared with experimental data obtained at a plant.

The nucleation fraction b is expected to be a complicated function of many factors: particle size distribution, bed hold-up and bed height, superficial gas velocity, local porosity, minimum fluidization porosity, spray injection velocity, and so on. It was argued that a strong dependence of b on bed height is expected in case the bed surface height and the spray nozzle height are about the same. This dependence of b on the bed height may cause instability and oscillatory behavior of the transient solution. Oscillatory behavior to a certain extent is typically found in practice, again showing the relevance of the model and its ability to describe phenomena encountered in reality. Given the importance of the nucleation fraction, consecutive work is going on to derive this parameter from discrete particle simulations of spray injection into a fluidized bed.

For the stability of the granulation process the slope of the parameter b as a function of fluid bed height appeared to be important. A critical value for this slope was derived from linear stability theory. Unstable (oscillatory) behavior occurs if the slope of the curve

at the actual steady state point is steeper than the critical slope value, otherwise the steady-state solution is stable. If the system is unstable, but does not violate the steady state condition, stability can be achieved, by increasing the height of the bed relative to the spray inlet. One possibility to increase the bed height relative to the spray inlet is to increase the spray mass flow. The stability properties of the system also improve if, relative to the minimum size of particles in the bed (L_0), the minimum product selection diameter L_1 is sufficiently decreased. If the product selection mechanism is switched off for all diameters, the model system is stable. These findings were confirmed by numerical simulations.

Appendix: Matrix coefficients

In this appendix we specify the matrix coefficients that determine the linear system for m_2' and m_3' in section 7. The coefficients arise from integrations of the exact solution for n' over the intervals $[r,1]$ and $[1,\infty[$. The coefficients equal

$$\begin{aligned}
a_1 &= -1+\gamma\Big(P(r,z,zr)-P(1,z,zr)+\\
&\quad P(1,z+\sigma,\sigma+zr)+\frac{\sigma}{z}(P(1,z+\sigma,z+\sigma)-P(1,\sigma,\sigma))\Big),\\
a_2 &= \beta\Big(P(r,z,zr)-P(1,z,zr)+\\
&\quad P(1,z+\sigma,\sigma+zr)+\frac{\overline{b}\sigma}{z}(P(1,z+\sigma,z+\sigma)-P(1,\sigma,\sigma))\Big),\\
a_3 &= \gamma\Big(Q(r,z,zr)-Q(1,z,zr)+\\
&\quad Q(1,z+\sigma,\sigma+zr)+\frac{\sigma}{z}(Q(1,z+\sigma,z+\sigma)-Q(1,\sigma,\sigma))\Big),\\
a_4 &= -1+\beta\Big(Q(r,z,zr)-Q(1,z,zr)+\\
&\quad Q(1,z+\sigma,\sigma+zr)+\frac{\overline{b}\sigma}{z}(Q(1,z+\sigma,z+\sigma)-Q(1,\sigma,\sigma))\Big),
\end{aligned}$$

where the functions P and Q are defined by ($z_1\neq 0$):

$$\begin{aligned}
P(\xi_1,z_1,z_2) &= \Big(\frac{\xi_1^2}{z_1}+\frac{2\xi_1}{z_1^2}+\frac{2}{z_1^3}\Big)e^{-z_1\xi_1+z_2},\\
Q(\xi_1,z_1,z_2) &= \Big(\frac{\xi_1^3}{z_1}+\frac{3\xi_1^2}{z_1^2}+\frac{6\xi_1}{z_1^3}+\frac{6}{z_1^4}\Big)e^{-z_1\xi_1+z_2},
\end{aligned}$$

while for $z_1=0$:

$$\begin{aligned}
P(\xi_1,0,z_2) &= -\tfrac{1}{3}\xi_1^3e^{z_2},\\
Q(\xi_1,0,z_2) &= -\tfrac{1}{4}\xi_1^4e^{z_2}.
\end{aligned}$$

The functions P and Q are defined such that the following equalities hold:

$$\begin{aligned}
\int_{\xi_1}^{\xi_2}\xi^2e^{-z_1\xi+z_2}d\xi &= P(\xi_1,z_1,z_2)-P(\xi_2,z_1,z_2),\\
\int_{\xi_1}^{\xi_2}\xi^3e^{-z_1\xi+z_2}d\xi &= Q(\xi_1,z_1,z_2)-Q(\xi_2,z_1,z_2).
\end{aligned}$$

This completes the specification of the characteristic equation of the linearized population balance equation.

References

[1] Drechsler, J., Peglow, M., Heinrich, S., Ihlow, M., Mörl, L., 2005. Investigating the dynamic behaviour of fluidized bed spray granulation processes applying numerical simulation tools. Chemical Engineering Science 60, 3817-3833.

[2] Heinrich, S., Peglow, M., Ihlow, M., Henneberg, M., Mörl, L., 2002. Analysis of the start-up process in continuous fluidized bed spray granulation by population balance modelling. Chemical Engineering Science 57, 4369-4390.

[3] Hounslow, M.J., Ryall, R.L., Marshall, V.R., 1988. A discretized population balance model for nucleation, growth and aggregation. A.I.Ch.E. Journal 34, 1821-1832.

[4] Kunii, D., Levenspiel, O., 1987. Fluidization Engineering. Robert Krieger Publishing Company Inc, Malabar.

[5] Lie, S.J., Shinnar, R., Katz, S., 1971. The stability and dynamic behavior of a continuous crystallizer with fines trap. A.I.Ch.E. Journal 17, 1459-1470.

[6] Peglow, M., Kumar, J., Heinrich, S., Warnecke, G., Tsotsas, E., Mörl, L., Wolf, B., 2007. A generic population balance model for simultaneous agglomeration and drying in fluidized beds. Chemical Engineering Science 62, 513-532.

[7] Radichkov, R., Mueller, T., Kienle, A., Heinrich, S., Peglow, M., Mörl, L., 2006. A numerical bifurcation analysis of continuous fluidized bed spray granulation with external product classification, Chemical Engineering Science 45, 826-837.

[8] Randolph, A.D., Beer G.L., Keener, J.P., 1973. Stability of the class II classified product crystallizer with fines removal. A.I.Ch.E. Journal 19, 1140-1149.

[9] Randolph, A.D., Larson, M.A., 1988. Theory of particulate processes. Academic Press, New York.

[10] Ramkrishna, D., 2000. Population balances: theory and applications to particulate systems in engineering. Academic Press, San Diego.

[11] Sherwin, M.B., Shinnar, R., Katz, S., 1969. Dynamic behavior of the well-stirred crystallizer with classified outlet. Chem. Eng. Progr. Symp. Ser. 95 (65), 75-90.

[12] Tan, H.S., Salman, A.D., Hounslow, M.J., 2006. Kinetics of fluidized bed melt granulation - II: Modelling of the net rate of growth. Chemical Engineering Science 61, 3930-3941.

Notation

A	bed bottom area
a_i	complex matrix coefficient
B	birth-term
B_0	multiplicator in birth-term
D	multiplicator in death-term
b	the nuclei generating fraction of the solute content of the spray
f	determinant function
G	particle diameter growth rate
H	Heaviside function
h	bed height (surface level)
h_{noz}	height of the spray nozzle location
Im	imaginary part of complex number
L	particle diameter
L_0	particle diameter of nuclei
L_1	threshold particle diameter corresponding to the sifter
m_2	second moment
m_3	third moment
n	particle number density function
p	dimensionless function of b and r
q	scaled (dimensionless) growth rate
r	diameter ratio L_0/L_1
Re	real part of complex number
s	fraction of particles ($L > L_1$) withdrawn from the bed per second
t	time
V	fluid bed volume
v	particle volume function
z	complex eigenvalue

Greek symbols

β	scaled (dimensionless) derivative of the function $b(h)$
γ	function of $\bar{b}$ and r
δ	delta-function
ϵ	bed porosity
Φ	volumetric mass flow corresponding to the solute content of the spray
ϕ	nondimensionalized Φ
ξ	nondimensionalized particle diameter
σ	nondimensionalized withdrawal rate
τ	nondimensionalized time

Superscripts

$'$	quantity is related to the perturbation eigenfunction in the linear analysis
$\bar{}$	quantity is related to the base steady state in the linear analysis